Carbohydrate Polymers 76 (2009) 68–73

Contents lists available at ScienceDirect

Carbohydrate Polymers

journal homepage: www.elsevier.com/locate/carbpol

Effect of citric acid and processing on the performance of thermoplastic starch/montmorillonite nanocomposites

Wang Ning [a,*], Zhang Xingxiang [a], Han Na [a], Bai Shihe [b]

[a] Institute of Functional Fibers, Tianjin Municipal Key Lab of Fiber Modification and Functional Fiber, Tianjin Polytechnic University, Chenglin Road 63#, Tianjin 300160, China
[b] College of Material Science and Chemical Engineering, Tianjin Polytechnic University, Tianjin 300160, China

ARTICLE INFO

Article history:
Received 4 September 2008
Received in revised form 16 September 2008
Accepted 18 September 2008
Available online 25 September 2008

Keywords:
Citric acid
Extrusion
Montmorillonite
Thermoplastic
Starch

ABSTRACT

A facile two steps extrusion processing conditions are used to prepare thermoplastic starch (TPS)/glycerol modified-montmorillonite (GMMT) nanocomposites. X-ray diffraction (XRD) and transmission electron microscopy (TEM) demonstrate glycerol can enlarge the *d*-spacing and destruct the multilayer structure of montmorillonite (MMT) effectively using high speed emulsifying machine (HSEM) in the first modification step. So the enlarged *d*-spacing and destructed platelets of MMT are favorable to form intercalated or exfoliated TPS/GMMT nanocomposites in the second melt extrusion processing. However, scanning electron microscopy (SEM) and XRD show the possible competition between TPS matrix and plasticizer for the intercalation between MMT layers can deteriorate the plasticization of TPS. In addition, citric acid (CA) can increase the plasticization of TPS and dispersion of MMT in nanocomposites effectively detected by fourier transform infrared (FT-IR) spectroscopy and SEM. At the same time, this facile processing conditions and CA can improve the mechanical properties and water vapor permeability (WVP) of TPS/GMMT nanocomposites obviously.

1. Introduction

In addition to being staple food, starch has recently gained interest as a renewable and biodegradable plastic, which is usually called thermoplastic starch (TPS) (Shogren, 1992). TPS can be made from amylose (poly-α-1, 4-D-glucan), amylopectin (poly-α-1, 4-D-glucan and α-1, 6-D-glucan) and theirs components by various techniques, such as solution casting (Cyras, Manfredi, Ton-That, & Vazquez, 2008) and thermoplastic extrusion processing (Ma, Yu, & Ma, 2005). Compared with solution casting, thermoplastic extrusion is a "green" and facile processing condition. Recently, a great deal of novel plasticizers, such as aliphatic amidediol (Zhang, Yu, Wu, & Ma, 2008), urea mixed with formamide (Ma et al., 2005) and ethylenebisformamide (Yang, Yu, Feng, & Ma, 2007) have been proved to improve the plasticization of starch effectively. Moreover, TPS combined with multiwall carbon nanotube or sodium chloride can be used as solid polymer electrolytes in previous reports (Ma, Yu, He, & Wang, 2007; Ma, Yu, & Wang, 2008). But the properties of TPS, especially the poor mechanical properties and water resistance limit the application of TPS in many areas. It can be improved by blending with synthetic polymers, such as poly(lactic acid), poly(caprolactone), poly(hydroxyalkanoate) and polyethylene (Wang, Yu, Ma, & Wu, 2007a; Wang, Yu, Chang, & Ma, 2008).

Moreover, montmorillonite (MMT) in nano-scale (below 5 wt%) can increase the mechanical properties, thermal stability and water resistance of TPS dramatically (Park, Lee, Park, Cho, & Ha, 2003; Wilhelm, Sierakowski, Souza, & Wypych, 2003). MMT is a kind of aluminum silicates classified as phyllosilicates, which is environmentally friendly and readily available in large quantities with relatively low cost (Ray & Bousmina, 2005). Subsequently some studies find only the plasticizer (water and glycerol) can intercalate into the narrow *d*-spacing of MMT effectively, but it is difficult for the macromolecular of starch (Zhang, Yu, Xie, Naito, & Kagawa, 2007). In order to achieve intercalated or exfoliated TPS/MMT nanocomposite, organo-modified MMT (OMMT) with wider *d*-spacing is used (Chen & Evans, 2005; Zhang et al., 2007). But the effect is not obvious because of the poor compatibility between hydrophilic TPS and hydrophobic OMMT. So the authors point out using hydrophilic modified MMT can be a promising way to further improve MMT exfoliation (Zhang et al., 2007).

In order to achieve high performance TPS/MMT nanocomposites, a facile two step extrusion processing conditions is used to prepare TPS/hydrophilic (glycerol) modified-MMT nanocomposites. In the presence of glycerol high speed emulsifying machine (HSEM) can enlarge the *d*-spacing and destruct the multilayer structure of MMT effectively in the first modification step. So the enlarged *d*-spacing and destructed platelets of MMT are favorable to form intercalated or exfoliated TPS based nanocomposites in the second melt extrusion step. However, the intense interactions,

* Corresponding author. Tel.: +86 22 24528144; fax: +86 22 24348894.
E-mail address: wang_n@yahoo.com.cn (N. Wang).

0144-8617/$ - see front matter © 2008 Elsevier Ltd. All rights reserved.
doi:10.1016/j.carbpol.2008.09.021

such as the H-bonding and the ion–dipole existed in this complex composite (Dean, Yu, & Wu, 2007; Wilhelm et al., 2003) can form the possible competition between TPS matrix and plasticizer for the intercalation between MMT layers. At the same time, it deteriorates the plasticization of TPS. In our previous works citric acid (CA) has been proved to increase the plasticization and melt processing properties of TPS effectively (Wang, Yu, & Han, 2007b; Wang et al., 2007a). So CA is also used as additive in this paper. In addition, the effect of CA and processing conditions on the performance of TPS/MMT nanocomposites are also studied.

2. Experimental

2.1. Materials

Cornstarch (12% moisture) was obtained from Langfang Starch Company (Langfang, Hebei, China). Glycerol and CA (analytical reagent) were purchased from Tianjin Chemical Reagent Factory (Tianjin, China). Na-MMT with a cation exchange capacity (CEC) of 90–100 mmol/(100 g) as an inorganic host material was supplied by Zhangjiakou Qinghe Chemical Plant (Zhangjiakou, Hebei, China).

2.2. Samples preparation

The contents of MMT were 1, 3, 5, 7 and 9 wt% based on starch, respectively. TPS/MMT nanocomposites were prepared in two steps processing conditions. In the first step, pristine MMT (PMMT) was mixed with glycerol (9000 rpm for 20 min) at a weight ratio of 10:3 by using of tank-type HSEM (Beijin, China). A pulp was obtained and named GMMT. The same weight glycerol and PMMT was manually mixed to form homogeneous phase as a contrast. The above two kinds of pulp, CA, complementary glycerol and starch were premixed (3000 rpm for 2 min) in the high speed mixer (Beijin, China) according to Table 1. The mixtures were stored in tightly sealed plastic bags for 24 h (a homogeneous mixture could be achieved) and then these mixtures were manually fed into the single screw plastic extruder SJ-25(s) (screw ratio L/D = 25:1, Shanghai, China) at a screw speed of 20 rpm. The temperature profile along the extruder barrel was 135–140–145–130 °C (from feed zone to die). The die was a round sheet with 3 mm diameter holes. TPS/MMT nanocomposites were stored airtight immediately. When the samples reached room temperature (about 20 °C), the extruded nanocomposites strips were pressed into sheets with model YITD71-454 Plastic Hydraulic Press (Tianjin, China) and cut into tensile bars with certain size and stored airtight under room temperature immediately. The properties test would go on after one week. TPS and CA (3 wt% based on starch) modification TPS (CTPS) were prepared by melt-processing of starch, glycerol and CA according to our previous work (Wang et al., 2007b), which were similar as the processing conditions of TPS/MMT nanocomposites.

2.3. Characterization

X-ray diffraction (XRD) of PMMT, GMMT and TPS/MMT nanocomposites were examined using a Rigaku D/Max 2500 V PC X-ray diffractometer (Rigaku, Tokyo, Japan) (40 kV, 100 mA) equipped with a Ni-filtered Cu radiation and a curved graphite crystal monochromator. The diffractometer was equipped with 1° divergence slit, a 0.16 mm receiving slit and a 1° scatter slit.

Scanning electron microscopy (SEM) and transmission electron microscopy (TEM) were used to characterize the micro-structure of nanocomposites. SEM was performed with a Philips XL-3 microscope (FEI, Hillsboro, OR). The samples were cooled in liquid nitrogen, and then broken. The fracture faces were coated with gold under vacuum for SEM observation. TEM was performed with a JEM-1200EX microscope (JEOL, Tokyo, Japan), operating at an accelerating voltage of 80 kV. PMMT and GMMT were dispersed in ethanol by sonication during 10 min at room temperature. TPS/MMT nanocomposites were sliced in liquid nitrogen with the Reichert-Jung Utracut E extrathin slicer. The thickness of the ultrathin slices was 50–70 nm.

Fourier Transform Infrared (FT-IR) Spectroscopy was obtained at 2 cm^{-1} resolution with BIO-RAD FTS3000 IR Spectrum Scanner (Hercules, USA). Typically, 64 scans were signal-averaged to reduce spectral noise. The samples were compressed to the sheet with the thickness of about 0.5 mm in the Flat Sulfuration Machine, tested by attenuated total reflection measurements.

According to the GB1040-79 standard of China, the tensile strength and elongation at break of nanocomposites were measured using a Testometric AXM350-10KN materials testing machine (Rochdale, Lancashire, UK). The crosshead speed was 100 mm/min. All samples were tested after being stored in an airtight container for one week after preparation. Each measurement was performed for five specimens (8 cm long × 3 mm diameter) and averaged.

Water vapor permeability (WVP) tests were carried out by ASTM method E96 (1996) with some modifications (Mali, Grossmann, Garcia, Martino, & Zaritzky, 2006). The films (about 0.5 mm thickness) were cut into circle shapes and sealed over with melted paraffin, stored in a desiccator at 25 °C. RH 0 was kept with anhydrous calcium chloride in the cell. And each cell was placed in a desiccator containing saturated sodium chloride to provide a constant RH 75%. Water vapor transport was determined by the weight gain of the permeation cell. Changes in the weight of the cell were recorded as a function of time. Slopes were calculated by linear regression (weight changes vs. time) and correlation coef-

Table 1
The symbols of TPS/MMT nanocomposites

Code	Starch (wt%)	Glycerol (wt%)	CA (wt%)	GMMT	
				Glycerol (wt%)	MMT (wt%)
TPS	100	30.0	–	–	–
TPS/GMMT1	100	26.7	–	3.3	1
TPS/GMMT2	100	20.0	–	10.0	3
TPS/GMMT3	100	13.3	–	16.7	5
TPS/GMMT4	100	6.7	–	23.3	7
TPS/GMMT5	100	–	–	30.0	9
CTPS	100	30.0	3	–	–
CTPS/GMMT1	100	26.7	3	3.3	1
CTPS/GMMT2	100	20.0	3	10.0	3
CTPS/GMMT3	100	13.3	3	16.7	5
CTPS/GMMT4	100	6.7	3	23.3	7
CTPS/GMMT5	100	–	3	30.0	9

ficients for all reported data were >0.99. The water vapor transmission rate (WVTR) was defined as the slope ($g\,s^{-1}$) divided by the transfer area (m^2). After the permeation tests, film thickness was measured and WVP ($gPa^{-1}\,s^{-1}\,m^{-1}$) was calculated as the following equation:

$$\mathrm{WVP} = \frac{\mathrm{WVTR}}{P(R_1 - R_2)} \cdot x \quad (1)$$

where P is the saturation vapor pressure of water (Pa) at the test temperature (25 °C), R_1, the RH in the desiccator, R_2, the RH in the permeation cell and x is the film thickness (m). Under these conditions, the driving force [$P(R_1–R_2)$] is 1753.55 Pa.

3. Results and discussion

Fig. 1 shows the XRD of PMMT, glycerol/PMMT manual mixture, GMMT and TPS/MMT nanocomposites. The d-spacing could be calculated from Bragg's formula.

$$d\text{-spacing} = n\lambda/(2\sin\theta) \quad (2)$$

where θ is the diffraction angle that gives the primary diffraction peak, and λ is the X-ray wavelength, n is an integer.

As shown in Fig. 1A PMMT exhibited a sharp peak (001) at $2\theta = 8.76°$ corresponding to the spacing of 1.01 nm between individual MMT layers. After MMT was manually mixed with glycerol, this peak shifted to 5.64°, which meant that the d-spacing of MMT expanded to 1.63 nm. It indicated that glycerol could intercalate and enlarge the layers of MMT effectively. After glycerol/PMMT mixture was processed with HSEM, the d-spacing of MMT was further expanded to 1.85 nm. At the same time, this peak became smaller than that of PMMT. It indicated that the high speed shearing force provided by HSEM could destruct the multilayer structure of PMMT in the presence of glycerol. It could be also detected by TEM testing.

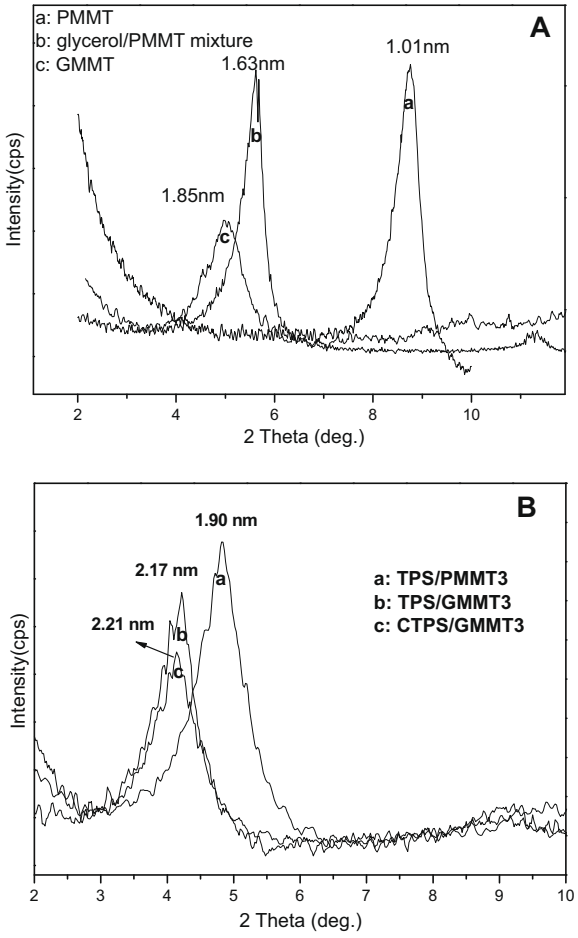

Fig. 1. XRD patterns of PMMT, glycerol/PMMT mixture, GMMT and TPS/MMT nanocomposites.

The enlarged d-spacing of GMMT was propitious to the intercalation of TPS. As shown in Fig. 1B, the d-spacing of MMT enlarged to about 2.2 nm in TPS/GMMT nanocomposites, which was wider than that of TPS/PMMT. Moreover, the peak (001) of MMT should become sharper after melt blending with TPS, which was ascribed to the orientation of MMT in the melt processing (Wilhelm et al., 2003). However, the peak (001) of MMT in TPS/GMMT nanocomposites decreased. It might indicate partial exfoliated TPS/GMMT also existed. At the same time, CA could further enlarge the d-spacing of MMT in CTPS/GMMT nanocomposites as shown in Fig. 1B. In the presence of CA the depolymerization of polysaccharide was propitious to the intercalation or partial exfoliation of GMMT.

To further confirm the nanostructure of TPS/MMT blends and verity the conclusions from XRD, TME was carried out. Fig. 2 shows the TME of PMMT, GMMT and TPS/MMT nanocomposites. As shown in TEM photograph of PMMT (Fig. 2A), PMMT mainly exhibited hexagon multilayer structure (deep color). The particle length was about 150 nm similar as previous report (Ray & Bousmina, 2005). Moreover, some irregular particles were also detected. After PMMT/glycerol mixture was processed with HSEM, only light gray fragment could be found (Fig. 2B). So HSEM could destruct the multilayer and platelet structure of PMMT obviously. In addition, it (GMMT) was propitious to the intercalation of TPS. Fig. 2C and D show the TEM images of TPS/PMMT3 and TPS/GMMT3, respectively. Compared with TPS/PMMT3, TPS/GMMT3 exhibited better dispersion and ordered intercalated structure. It ascribed to the wider d-spacing and the smaller platelet of GMMT.

As previous report, TPS was consisted of a molecular network of semicrystalline amylose and amylopectin with some granular fragments, and the mechanical properties of TPS also depended on the crystallinity of the constituting polymers (van Soest, Hulleman, de Wit, & Vliegenthart, 1996). After MMT was hydrophilic modified by glycerol in the first step, it was propitious to form intercalated structure TPS/GMMT nanocomposites. However, a great deal of residual A-type crystallinity could be detected in both TPS/PMMT and TPS/GMMT nanocomposites as shown in Fig. 3. It is proved that MMT deteriorated the plasticization of TPS and led to most residual starch granules embed in partly destructed polysaccharide network. Because the intense interactions existed between plasticizer and MMT layers could decrease the H-bonding interaction between plasticizer and starch. When 3 wt% CA was added to this complex composite, the plasticization of TPS in CTPS/MMT nanocomposites could be improved dramatically. As shown in Fig. 3 the intense A-type crystallinity peak nearly disappeared in CTPS/GMMT3 nanocomposites. The effect of CA on the plasticization of TPS could be also proved by morphological analysis.

As shown in Fig. 4A TPS presented a continuous phase and no residual starch granule could be found on the fractured surfaces. After blending with GMMT in one step extrusion, many residual starch granules existed on the fracture surface of TPS/GMMT nanocomposites (Fig. 4B). It ascribed to the H-bonding interaction existed between hydroxyl groups of MMT and plasticizer (Wilhelm et al., 2003); moreover, the ion–dipole interaction could also form between MMT and plasticizer as previous reports (Dean et al., 2007). Compared with polysaccharide network, small molecular plasticizer could intercalate into MMT layers easily. So MMT layers could shield the interaction between starch and plasticizer, especially in TPS/GMMT nanocomposites. In addition, the plasticization of TPS in TPS/GMMT nanocomposites was poor. In the presence of CA (Fig. 4C), the fracture surfaces of CTPS/GMMT3 became smooth.

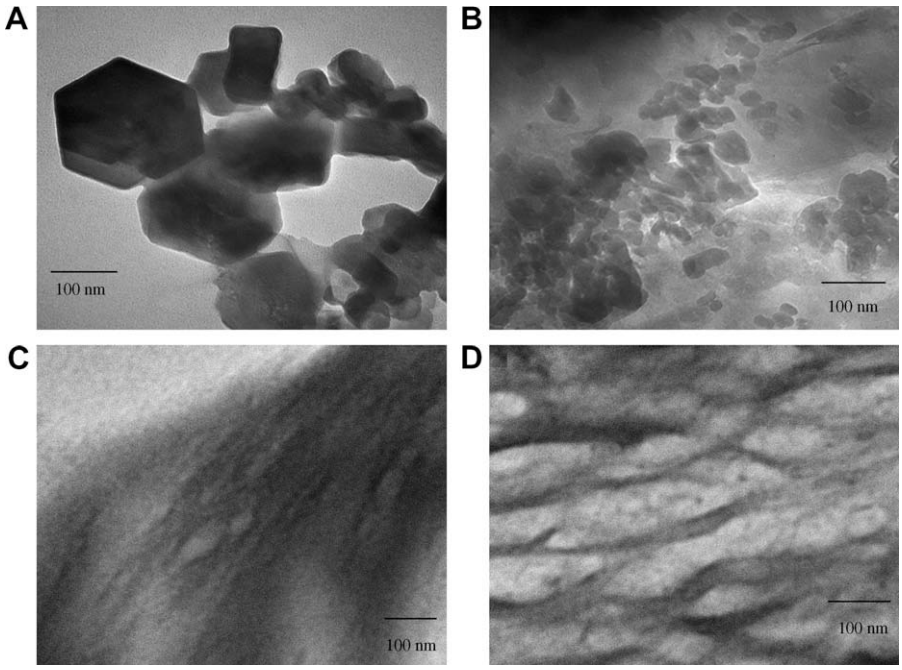

Fig. 2. The TEM photographs of PMMT, GMMT, TPS/PMMT and TPS/GMMT. (A) PMMT, (B) GMMT, (C) TPS/PMMT4, (D) TPS/GMMT4.

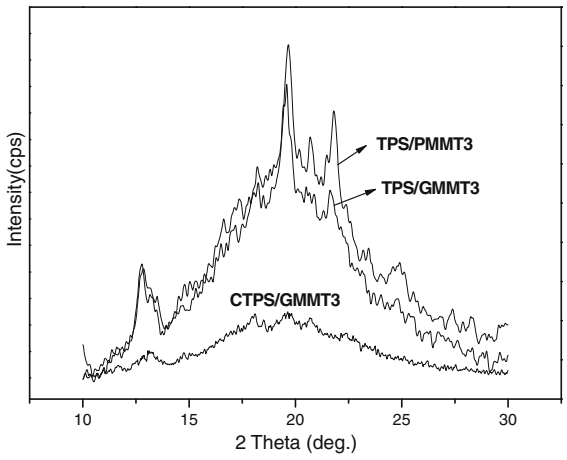

Fig. 3. XRD patterns of TPS/PMMT, TPS/GMMT and CTPS/GMMT nanocomposites.

No residual starch granules could be detected. This was attributed to acidic CA could accelerate the fragmentation and dissolution of starch granule. The destroyed starch structure can be permeated by plasticizer easily (Wang et al., 2007b). So high plasticization and dispersion TPS/MMT nanocomposites could be achieved. It could be also proved in FT-IR spectroscopy study.

FT-IR analysis of the composites could identify the interactions in glycerol/PMMT manual mixture, GMMT and TPS/MMT nanocomposites. On the basis of the harmonic oscillator model, it concluded that the lower the peak frequency the stronger was the interaction (Pawlak & Mucha, 2003). Fig. 5A shows that the OH stretching peak, ascribed to the hydroxyl groups, appeared at 3300–3500 cm^{-1}, while the O–C stretching peak, which was ascribed to C–OH groups, appeared at about 1100 cm^{-1}. These two characteristic peaks (3373 and 1095 cm^{-1}) were situated at lower wavenumber in GMMT than those (3382 and 1109 cm^{-1}) in glycerol/MMT manual mixture. It indicated that plasticizer could form intense H-bonding interaction with the hydroxyl groups of MMT molecules during the first MMT hydrophilic modification processing. So it was advantageous to the intercalation of glycerol into MMT layers.

Fig. 5B shows the FT-IR spectrum of TPS/MMT nanocomposites. In the fingerprint region of FT-IR spectrum of TPS, three characteristic peaks appeared between 1200 and 900 cm^{-1}, attributed to C–O bond stretching of starch (Fang, Fowler, & Tomkinson, 2002). The characteristic peak near 1150 cm^{-1} was ascribed to C–O bond stretching of the C–O–H group in starch, while two peaks at 1080 and 1020 cm^{-1} were attributed to C–O bond stretching of the C–O–C group in the anhydroglucose ring. Compared with TPS/PMMT, the corresponding characteristic peaks of TPS/GMMT nanocomposites shifted to lower wavenumber. Especially, in CTPS/GMMT nanocomposites with 3 wt% CA showed the lowest wavenumber. It indicated that CA could increase the interaction in this complex nanocomposites.

The mechanical properties of TPS were very poor as previous reports (Ma et al., 2005; Shogren, 1992). So it was necessary to take reinforced modification. Fig. 6 shows the tensile properties of TPS and TPS/MMT nanocomposites with different MMT contents, which were tested after being stored at the airtight container for one week since the preparation. It could be found that the tensile strength of TPS/MMT nanocomposites generally improved with increasing MMT content, but just the reverse for elongation at break. Moreover, the tensile strength of TPS/GMMT was higher than CATPS/GMMT nanocomposites when MMT content below 3 wt%. It could be attributed to most of residual starch granules embedded in an entangled matrix of amylase and amylopectin networks (as shown in Fig. 5B) which increased the stiffness of the TPS/MMT nanocomposites by physical crosslink. However, the high content MMT (above 3 wt%) could not only deteriorate the plasticization of TPS, but also destructed the continuity of TPS matrix. So the tensile strength of TPS/GMMT became lower than CATPS/GMMT nanocompostes when MMT content above 3 wt%. At the same time, CATPS/GMMT nanocompostes showed better elongation at break. CA could increase the plasticization of TPS had been proved in previous studies (SEM, XRD and FT-IR analysis). So the enhancement in mechanical properties of CATPS/

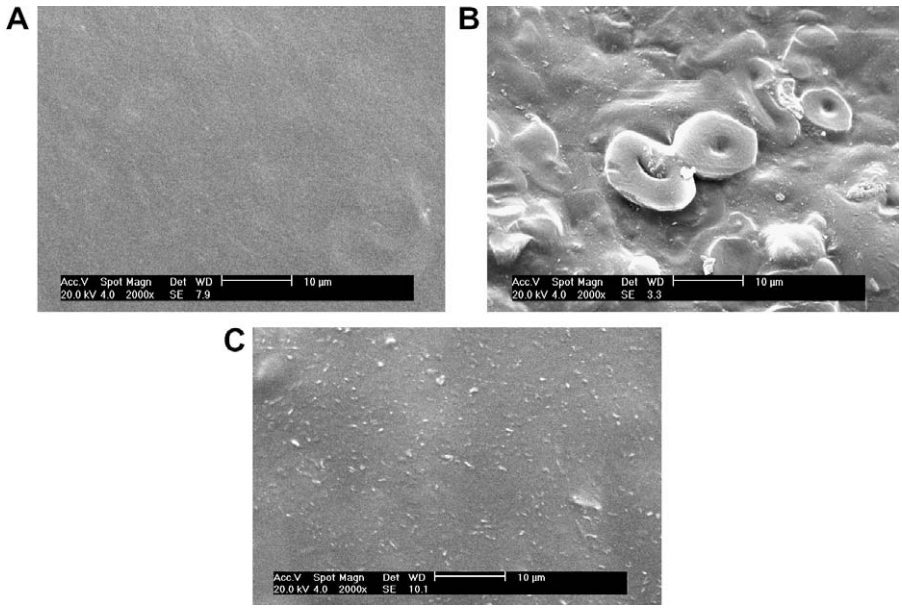

Fig. 4. The SEM photographs of TPS and TPS/MMT nanocomposites. (A) TPS, (B) TPS/GMMT3, (C) CTPS/GMMT3.

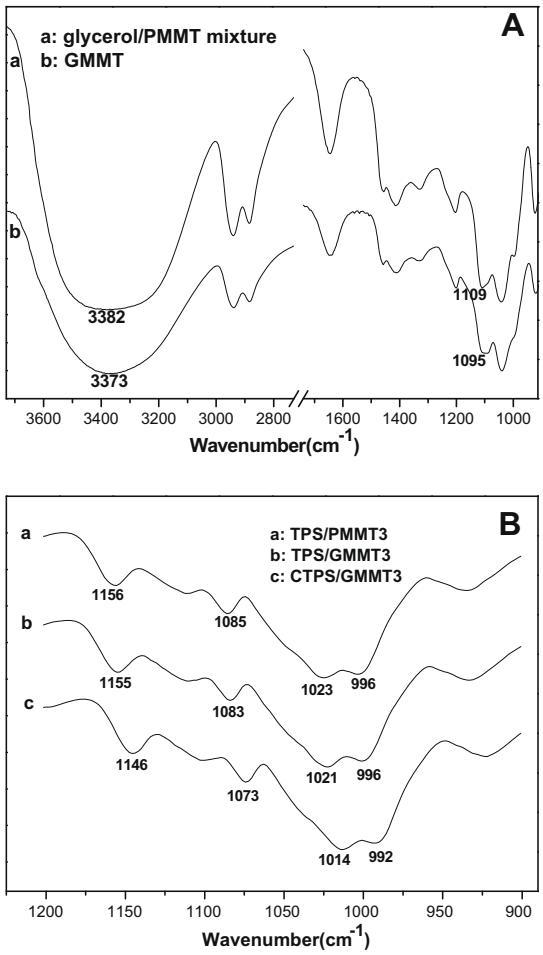

Fig. 5. FT-IR spectra of glycerol/PMMT mixture, GMMT and TPS/MMT nanocomposites.

GMMT nanocompostes could be attributed to the good affinity between highly plasticized TPS and hydrophilic modified MMT.

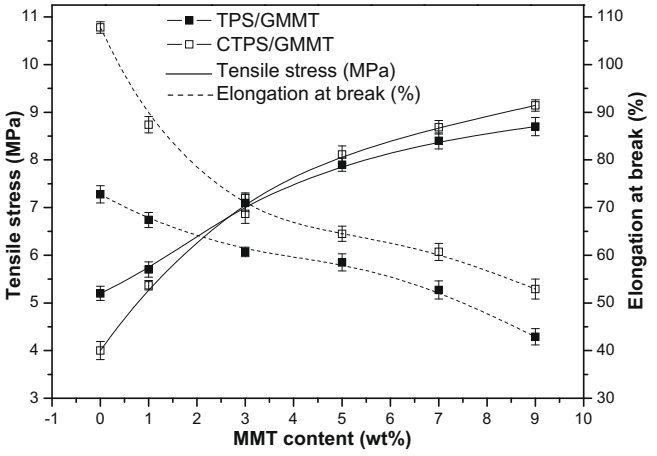

Fig. 6. The mechanical properties of TPS/GMMT nanocomposites.

As packaging material, WVP of the film should be as low as possible. As shown in Fig. 7, WVP in TPS/MMT nanocomposites decreased with increasing MMT contents. Because of starch molecular with a great deal of hydrophilic hydroxyl groups, water vapor could permeate TPS film easily (the highest WVP value at about 5.0×10^{-10} gm^{-1} s^{-1} Pa^{-1}). In the presence of MMT a maze or "tortuous path" structure could form in polymer matrix after blending with MMT, which blocked the normal water channels (Ray & Okamoto, 2003). So MMT could improve the water resistance of TPS effectively. Moreover, the exposed hydroxyl groups of starch shielded by highly dispersive MMT layers also decreased the water sensitive of TPS. Compared with TPS/PMMT, WVP value of TPS/GMMT nanocomposites obviously decreased at the same MMT content, especially in CTPS/GMMT nanocomposites. The WVP of CTPS/GMMT5 decreased to about 2.0×10^{-10} gm^{-1} s^{-1} Pa^{-1}.

4. Conclusion

In this paper CA and a facile method were used to prepare highly plasticized and dispersive TPS/MMT nanocomposites. Glycerol could increase the *d*-spacing and destruct the multilayer struc-

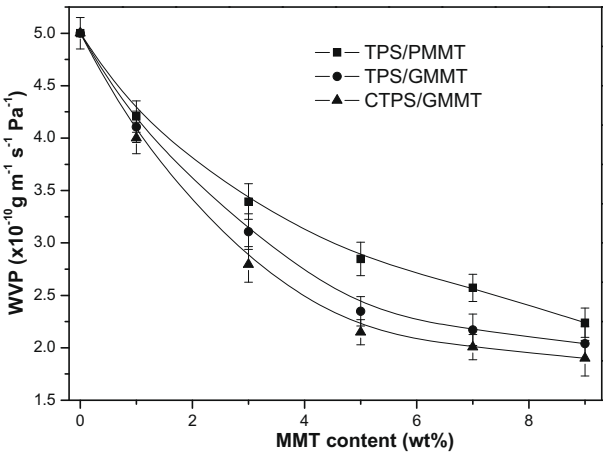

Fig. 7. The effect of MMT contents on WPV of TPS/MMT nanocomposites.

ture of MMT dramatically after processed with HSEM. The enlarged *d*-spacing and destructed platelets were propitious to form intercalated structure TPS/MMT nanocomposites during the melt extrusion processing. But the intense interactions (the H-bonding and the ion–dipole) existed in this complex nanocomposites could deteriorate the plasticization of TPS. In the presence of CA, the plasticization of TPS in CTPS/GMMT nanocomposites was improved dramatically. The high plasticization of TPS and good dispersion of GMMT in TPS matrix exerted an important influence on the improvement the mechanical properties and WVP value of CTPS/GMMT nanocomposites.

References

Cyras, V. P., Manfredi, L. B., Ton-That, M. T., & Vazquez, A. (2008). Physical and mechanical properties of thermoplastic starch/montmorillonite nanocomposite films. *Carbohydrate Polymers, 73*, 55–56.

Chen, B. Q., & Evans, J. R. G. (2005). Thermoplastic starch-clay nanocomposites and their characteristics. *Carbohydrate Polymers, 61*, 455–463.

Dean, K., Yu, L., & Wu, D. Y. (2007). Preparation and characterization of melt-extruded thermoplastic starch/clay nanocomposites. *Composites Science and Technology, 67*, 413–421.

Fang, J. M., Fowler, P. A., & Tomkinson, J. (2002). The preparation and characterisation of a series of chemically modified potato starches. *Carbohydrate Polymers, 47*, 245–252.

Ma, X. F., Yu, J. G., & Ma, Y. B. (2005). Urea and formamide as a mixed plasticizer for thermoplastic wheat flour. *Carbohydrate Polymers, 60*, 111–116.

Ma, X. F., Yu, J. G., He, K., & Wang, N. (2007). The effects of different plasticizers on the properties of thermoplastic starch as solid polymer electrolytes. *Macromolecular Materials and Engineering, 292*, 503–510.

Ma, X. F., Yu, J. G., & Wang, N. (2008). Glycerol plasticized- starch/multiwall carbon nanotube composites for electroactive polymers. *Composites Science and Technology, 68*, 268–273.

Mali, S., Grossmann, M. V. E., Garcia, M. A., Martino, M. N., & Zaritzky, N. E. (2006). Effects of controlled storage on thermal, mechanical and barrier properties of plasticized films from different starch sources. *Journal of Food Engineering, 75*, 453–460.

Park, H. M., Lee, W. K., Park, C. Y., Cho, W. J., & Ha, C. S. (2003). Environmentally friendly polymer hybrids - Part I - Mechanical, thermal, and barrier properties of thermoplastic starch/clay nanocomposites. *Journal of Materials Science, 38*, 909–915.

Pawlak, A., & Mucha, M. (2003). Thermogravimetric and FTIR studies of chitosan blends. *Thermochimica Acta, 396*, 153–166.

Ray, S. S., & Bousmina, M. (2005). Biodegradable polymers and their layered silicate nano composites: In greening the 21st century materials world. *Progress in Materials Science, 50*, 962–1079.

Ray, S. S., & Okamoto, M. (2003). Biodegradable polylactide and its nanocomposites: Opening a new dimension for plastics and composites. *Macromolecular Rapid Communications, 24*, 815–840.

Shogren, R. L. (1992). Effect of moisture-content on the melting and subsequent physical aging of cornstarch. *Carbohydrate Polymers, 19*, 83–90.

van Soest, J. J. G., Hulleman, S. H. D., de Wit, D., & Vliegenthart, J. F. G. (1996). Changes in the mechanical properties of thermoplastic potato starch in relation with changes in B-type crystallinity. *Carbohydrate Polymers, 29*, 225–232.

Wang, N., Yu, J. G., Chang, P. R., & Ma, X. F. (2008). Influence of formamide and water on the properties of thermoplastic starch/poly(lactic acid) blends. *Carbohydrate Polymers, 71*, 109–118.

Wang, N., Yu, J. G., Ma, X. F., & Wu, Y. (2007a). The influence of citric acid on the properties of thermoplastic starch/linear low-density polyethylene blends. *Carbohydrate Polymers, 67*, 446–453.

Wang, N., Yu, J. G., & Han, C. M. (2007b). Influence of citric acid on the properties of glycerol-plasticised Cornstarch extrusion blends. *Polymers & Polymer Composites, 15*, 545–552.

Wilhelm, H. M., Sierakowski, M. R., Souza, G. P., & Wypych, F. (2003). Starch films reinforced with mineral clay. *Carbohydrate Polymers, 52*, 101–110.

Yang, J. H., Yu, J. G., Feng, Y., & Ma, X. F. (2007). Study on the properties of ethylenebisformamide plasticized corn starch (PTPS) with various original water contents of corn starch. *Carbohydrate Polymers, 69*, 256–261.

Zhang, J. S., Yu, J. G., Wu, Y., & Ma, X. F. (2008). Synthesis of aliphatic amidediol and used as a novel mixed plasticizer for thermoplastic starch. *Chinese Chemical Letters, 19*, 395–398.

Zhang, Q. X., Yu, Z. Z., Xie, X. L., Naito, K., & Kagawa, Y. (2007). Preparation and crystalline morphology of biodegradable starch/clay nanocomposites. *Polymer, 48*, 7193–7200.